Energy efficiency of the High-Current Diode under the Blow-up Mode Evolution in the Anode

A. Adamenko[1, *], V. Novikov[1, *], V. Levchenko[1], V. Prokopenko[1, 2], A. Shapoval[1, 2], A. Pashchenko[1, 2], V. Petukhov[1, 2], I. Shapoval[1, 2]

[1]Proton – 21, Kyiv, Ukraine
[2]NSC KIPT, Kharkiv, Ukraine
[*]Corresponding author

A B S T R A C T

The results of experimental studies of energy fluxes released during the diode target blow-up initiated by a high-current relativistic electron beam are presented in the paper. The energy of target explosion products required for realization of the observed diode structural elements deformation is being estimated. Measurements of the target explosion products parameters and finite-element modeling of the mechanical deformation of the cathode system elements show an energy release during the target explosion that far exceeds the energy input.

1. Introduction

Nuclear fusion reactions are the most abundant source of energy in the universe, fueling stars and galaxies, and generating all elements heavier than hydrogen and helium.

However, recreating this process on Earth is currently a resource-intensive endeavor and remains primarily a scientific pursuit rather than an industrial technology. The most successful methods to date involve thermonuclear projects using tokamaks and superpower lasers ([1]-[2]), as well as inertial confinement using pulsed beams, such as the Sandia Z-pinch [3]. Another approach, inertial electrostatic confinement [4] with virtual electrodes (see, [5-6]), is capable of producing fusion reactions but is less energy-efficient than laser fusion.

In the Proton-21 laboratory, progress in solving the problem of inertial nuclear fusion has been made by applying the principles of self-organization and control of complex systems using high-current relativistic diodes. The latest Proton-21 facilities use a driver structure similar to the Sandia Z-pinch, but with a significantly lower initial energy (of the order of 30 kJ) and a special design of the target and reactor [7,8] design to simulate fusion reactions that occur in collapsing stars and supernova explosions [9,10].

The basic elements of the concept of controlled self-organizing fusion were published in a book edited by S. Adamenko et al [7 as well as in papers [11]-[19].

To date, since 1999, Proton-21 has accumulated a powerful database of experimental results, some are described in [7] and [22]-[25], and the facilities themselves were protected by an international patent by S. Adamenko [8].

The first units developed in the laboratory (units of RVD type) were created on the basis of plasma opening switch. They were able to produce electron beam pulses with durations of up to 40 nanoseconds, with the electron energy reaching up to 500 keV, and with the energy of electron beam during the pulse as high as hundreds of joules with the energy in primary capacitive storage up to 5 kJ.

When the electron beam impacted the target anode, it initiated a nonlinear density wave that moved from the surface to the optical center of the target with hyperbolic growth blow-up mode. This caused the explosion of the target in the central region, with the products scattered in all directions at high velocities of about 10^6 cm/s or more.

Experiments in the Proton-21 laboratory were always accompanied by online and offline measurements, including

voltage and current pulses in the diode, radiation in the optical range, as well as X-ray and gamma-ray radiation.

In the offline mode, for example, track [7,22-23] and mass spectroscopic measurements were conducted [16].

During the experiments at these units, the first results on self-organizing nuclear fusion in targets (anodes) made of various materials were obtained, and fusion products of both light and heavy elements were studied experimentally [7,20,25]. The mass of the target involved in the fusion processes in these experiments did not exceed a few milligrams.

The next two units of Proton-21 laboratory, SING and ShAD with 30 kJ up to 55 kJ in primary energy storage, were designed to sequentially increase target mass and energy release in fusion reactions initiated by the impact of a high current pulsed electron beam on the target surface.

An increase in the mass of the target involved in the synthesis was possible to achieve both by increasing the power of the units, and accordingly, the energy of the pulsed electron beam from values of about kJ in SING to values of about 10 kJ in ShAD, as well as by increasing the radius of the target while maintaining the critical current density on the target. At the same time, in ShAD, the mass of the part of the target involved in the synthesis approached values of the order of a gram.

In each experiment using the last generation units in the result of the impact of an electron beam with energies up to 10 kJ towards the surface of a target with a radius of millimeters, the energy release processes were initiated in blow-up mode (on blow-up mode, see, for example, [7,16,21]) and an explosion occurred in the central region of the target.

The anode-target explosion products and energy fluxes were dispersed from the central region and were observed by optical methods including: Doppler's spectral line broadening, time-of-flight method and high shutter speed recording of the explosion process and product dispersal.

The measurements trace the velocities of the product dispersal speed with values of the order of 10^7 cm/s. The products of target explosion deformed the cathode system. This mechanical work of deformation was estimated as a result of mathematical modeling of the explosion products' pressure pulses impact on the cathode system.

Both simulation results and optical measurements lead to explosion product flux energy estimations in values of the order of hundreds of kJ.

The paper presents the results of these studies showing high energy efficiency of Proton-21's Q units (ratio of energy released in the process of target detonation to the primary storage energy), which is higher than 10.

2. On the general concept of nuclear fusion control in the anode of a high-current diode

In the first Proton-21 installations, a controlled collective synthesis was achieved in a target made of various materials and register the transmutation of target nuclei into a wide range of newly formed elements in macro quantities (about a milligram of elements resulting from transmutation at the first installations). The block diagram of the latest modifications of the installations (ShAD type installations) is shown in Fig. 1.
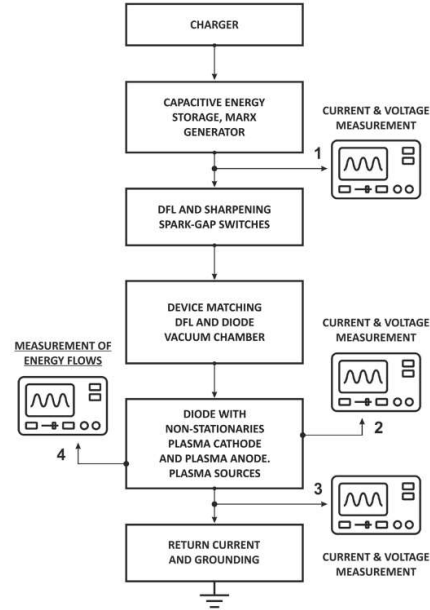
Fig. 1. *Block diagram of the ShAD installation. Areas for measuring currents and voltages in the installation are marked. The energy of the Marx generator capacitive storage (about 30 kJ, the potential difference across the capacitors U_0 is less than 100 kV (usually about 65 kV).*
(1) The voltage at the output of the pulse storage U_s is about 950 kV.
(2) The beam current in the diode for different experiments was on average from 250 kA to 400 kA (beam energy is about 12 kJ).
(3) The current at the diode output after the target explosion was about MA and higher (current energy is about 100 kJ).
*(4) The energy flux of particles and radiation from the explosion region is about several hundred kJ.*

As shown in the block diagram, a high voltage pulse is applied to the vacuum gap of the diode's plasma cathode-anode system. The distance between the cathode itself and the anode consists of the region occupied by the plasma moving in the gap and the contracting vacuum region.

The active resistance of the vacuum gap of the diode at the beginning of the process is large (a value of the order of a thousand ohms and eventually drops to zero when the gap disappears), and the resistance of the plasma conductor grows from zero to a maximum value, which is equal to the resistance of this plasma conductor with a length equal to the initial gap between the cathode and an anode.

The current pulse is determined by the high voltage pulse across the diode and the diode impedance as a function of time. Obviously, the diode impedance is controlled by the temperatures of the background and discharge plasma and the time of their appearance in the cathode–anode gap. The imaginary part of the impedance depends nonlinearly on the characteristic times of the process and is controlled by the shape of the voltage and current pulses. The current in a diode

is determined by the modulus of its impedance.

A typical diode impedance versus time is shown in FIG. 2, while the corresponding voltage and current pulses in FIG. 3.
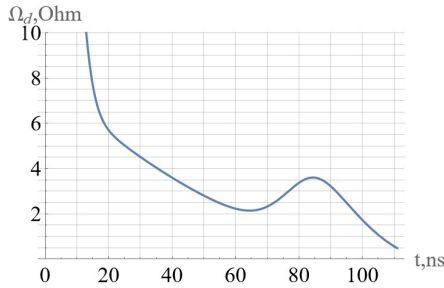

Fig. 2. Typical diode impedance versus time. *The active resistance of the diode is equal to the sum of the vacuum gap resistance* $\Omega_{acvc} \approx \dfrac{1}{U^{1/2}} \dfrac{d_{accm}^2}{S_{top}}$ *for the value of the cathode-anode gap equal to* d_{accm} *and resistance of the plasma conductor* $\Omega_{pl} \sim l_{pl}(t)$.
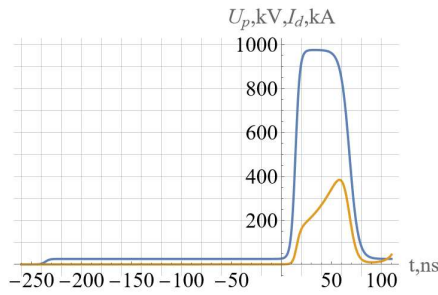
Fig.3. Characteristic view of the current pulse in the diode, shown together with the high voltage pulse. *The characteristic shape of the current pulse is determined by: the time shift of the current pulse maximum from the voltage maximum, the duration of the current pulse, the duration of the leading edge of the current pulse, the amplitude of the current pulse. The maximum value of the electron beam power is about 10^{12} Watts*
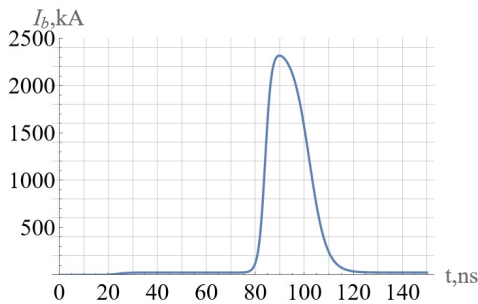
Fig.4. Characteristic view of the current after leaving the region of the exploding anode (in the region of the return conductor). *The effect of charge reset effect in a diode with a virtual cathode is observed [5]. The current amplitude is several times greater than the current amplitude in the diode and in some experiments exceeded 2.5 MA. The current energy for the entire time after the explosion reached 100 kJ, which exceeded the energy (about 30 kJ) contained in the primary storage*

The necessary conditions for synthesis in the target are achieved under the impact of an electron beam on the surface of the target anode. When a pulsed electron beam is focused on the anode-target surface, the beam electrons penetrate into the material to a certain depth in mkm $l_\varepsilon\left(U_{kV}, \rho\right) \approx k_{coll}(j) 0.6\, U_{kV}^{5/3} \rho^{-1}$, which depends on the density ρ of the anode substance in grams per cubic centimeter, the electron energy corresponding to the potential U_{kV} in kilovolts and depending on the current density $0.3 \le k_{coll}(j) \le 1$ ($k_{coll}(j) \approx 1$ at low current densities and $k_{coll}(j) \approx 0.3$ at high current densities).

Thus, it can be assumed that a drift space is realized between the anode surface and the surface near which the electrons stop inside the target. Electrons flying into this layer form a potential distribution with a minimum in a certain region (virtual electrode region) and beam electrons appear, reflected from this region.

The dynamics of the energy flow of the electron beam and the potential distribution in the anode under the action of a high voltage pulse is determined by the parameter $q_a\left(U_{kV}, j_{MA}, \rho\right) \approx 177.9 k_{coll}^2 j_{MA}(t) U_{kV}^{11/6}(t) \rho^{-2}$.

If the current density $j_{MA}(t)$ in mega Amperes per square centimeter on the target and the electron energy at time t_1 satisfy the condition q>q$_{cr1}$, then a system of virtual electrodes appears near the anode surface, in which the driver energy accumulates up to a certain time t_2 in the voltage drop interval external impulse. This moment of time is determined by the condition q<q$_{cr2}$ [5].

The critical values q$_{cr1}$ and q$_{cr2}$ decrease with an increase in the resistivity ρ_Ω of the target anode material approximately by the relations $q_{cr1} = k_\Omega 16/9$, $q_{cr2} = k_\Omega 8/9$, $k_\Omega \approx \exp(-\alpha \rho_\Omega)$ [6].

Thus, after the accumulation of energy of the pulse action in the target body, a nonlinear density wave is initiated and evolves, moving from the surface to the optical center of the target ([7]) in the implosion mode with sharpening (see Fig. 4).

There are some qualitative differences between a nonlinear wave in the concept of self-organizing fusion and in the scheme of inertial synthesis.

In the concept of coherent inertial fusion, the wave front is in a coherently correlated state and naturally separates the regions of the "fuel" entering the wave and the combustion products remaining behind the trailing wave front.

With a sufficiently rapid increase in the power of the driver action on the target surface, the dynamics of plasma-field structures occurs in the blow-up mode [21,16], in which the density of the structure grows in a self-consistent explosive manner under the conditions of electron collapse [28] and in a coherently correlated state [14].

This quasi-potential structure resembles the Bussard-Farnsworth reactor of inertial electrostatic confinement [4], transferred to a highly non-stationary regime of a plasma-field structure moving with self-increasing energy towards the center of the target [7,13].
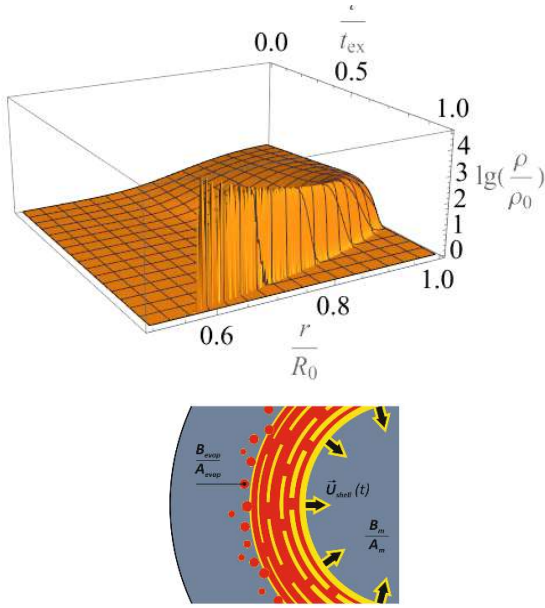
Fig. 5. Nonlinear wave propagating from the surface to the optical center of the target in the implosion blow-up mode. *The wave front has a fractal structure [7,13] in a coherently correlated state, through which the substance of the medium is filtered and new nuclei are formed at the trailing wave front. The estimates for density of nonlinear wave were performed in the hydrodynamic approximation using the Lagrangian particle method.*

High accelerations at the wave front in the blow-up mode implosion lead to the fact that the interacting particles in the region of the wave front end up in a coherently correlated state (CCS). In a coherently correlated state ([14],[27]), at the wave front, already on the way from the surface to the center of the target, conditions are created for suppressing the Coulomb barrier and for fusion to occur during the dynamic interaction of all particles with each other at extreme electron densities and accelerations in large volumes of the wave front in a solid target, similar to fusion reactions in collapsing stars [9,10].

The complexity of nuclear fusion technology is due to the fact that at relatively low energies of interacting particles, the probabilities of fusion processes and the transparency of the Coulomb barriers $\sim \exp\left(-2S_{eff}/\hbar\right)$ turn out to be negligible values due to smallness of Planck's constant $\hbar$.

In non-inertial systems with an explosive growth of accelerations, an explosive growth coefficient of coherence and correlations κ_{ph} at the phase space takes place, such systems become coherently correlated, and rapidly growing accelerations are accompanied by the appearance of an explosively growing factor multiply with Planck's constant.

For estimates, we can accept the fact that the properties of the CCS can be understood by introducing the effective Planck constant $\hbar_{eff} = \hbar \dfrac{1}{\sqrt{1-\kappa_{ph}^2}}$ [14] in accordance with the Schrödinger–Robertson relations.

Considering that in estimates of the probability of processes involving the Coulomb barrier, the constant appears in the exponential, it becomes clear that the probability of synthesis in the CCS can be increased by tens of orders of magnitude. It was shown in [7,18, 19] that the analysis of a dynamic system formed by particles of a substance involved in a nonlinear wave leads to a general conclusion about the existence of the possibility of initiating self-organization processes in this system, which results in the synthesis of a spectrum of elements as a result of the "life activity" of the evolving system on the way from its inception to its collapse.

The abundance of elements in the synthesis products depends on the degree of nonequilibrium and correlations in the synthesis process. The features of the spectrum of synthesis products are clearly manifested if the elements of synthesis are arranged in descending order of their prevalence. The resulting distribution has a degree-like form of the Zipf-Mandelbrot law with the spectrum index s, similar to the spectrum abundance of elements under collisions of heavy ions [29]. Distributions of this type in multifragmentation can follow from the non-extensive Tsallis statistics [28].

After averaging the binding energy of the fusion products over the distribution function, the dependence of the average binding energy per nucleon on the index of the product spectrum (see Fig. 6.)
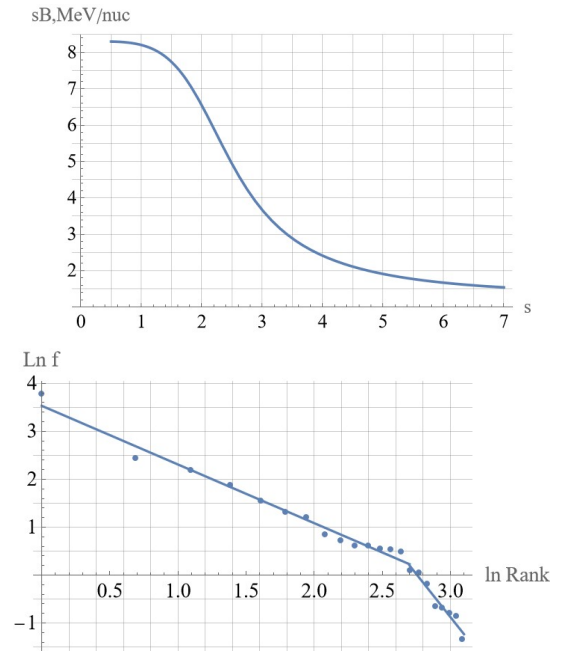
Fig. 6. The dependence of the average binding energy per nucleon on the index of the product spectrum s (top). Typical Zipf-Mandelbrot distribution for the abundance of synthesis products from the experimental results of optical measurements (bottom)

On the Fig. 6 also shows (bottom) the Zipf-Mandelbrot distribution of the abundance for the products of the synthesis, obtained from experimental data (the data corresponds to the index $s = 1.22$). For most experiments, the value of the index lies in the interval 1.2<s<1.5

The number of nucleons involved in the fusion process is determined by the target mass and driver parameters, and their typical number in experiments at our facilities lies in a wide range from 10^{19} to 10^{21}. For typical targets made of boron, titanium, and lead, the average energy yield of reactions is hundreds of KeV per nucleon, so the total energy yield in our experiments lies in the range of megajoules. The results of studies on the shell structure of nuclei [30] and the fractal structure of nuclear matter [31] at densities lower than the density of nuclei under normal conditions can be used to explain the existence of superheavy stable elements in theory and experiments [7,32].

In such a case, in order to produce sufficient power output, the fusion fuel elements do not have to be the lightest elements. Fuel can be almost any material.

One of the accompanying phenomena of coherent synthesis is a significant decrease in the radioactivity of the reaction products with initially radioactive targets. This can provide a means to decontaminate radioactive waste and, more generally, to convert virtually any toxic or unusable material into sustainable and safe items.

3. The SING unit and mathematical modeling of deformation of its cathode system

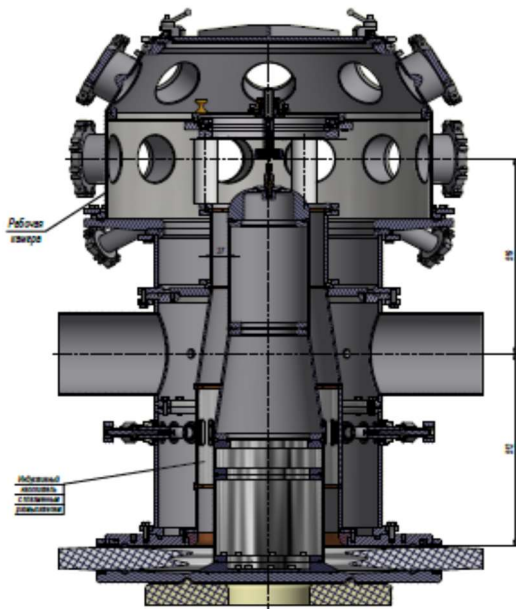The SING unit has become the result of the development of RVD type units, shown in Fig.7

Fig.7. Sketch of SING unit with plasma disconnectors and diode

A cathode system (electron beam source) and a target anode are located in the vacuum chamber (see Fig. 8). The cathode system consists of a copper rod on which a piece of plastic tube (PT) is put. The anode is made as a metal cylinder. 3 mm in diameter with a rounded end.
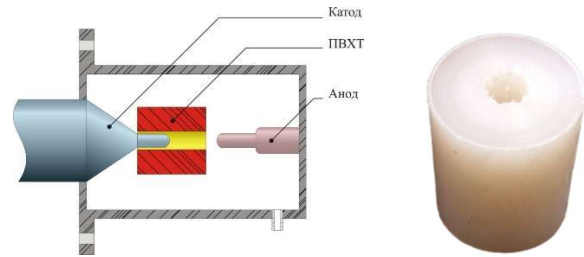

Fig. 8. Diagram of PT arrangement in diode and a picture of initial PT

The SING unit's capacitive storage has a capacity of 1.875 µF and is usually charged to a potential difference of no more than 70 kV, i.e., the initial stored energy is about 50 kJ. The energy of explosion products, flying out from the center of the target is clearly manifested by mechanical effect produced by their short impact on the structural elements and, in particular, on PT, which is being turned inside out on the cathode rod by this impact. The energy required for this is evaluated in the result of mathematical modeling of these processes by the finite element method [26].

The main evaluations were obtained for the PT model in the elasticity approximation of its shape change processes within the framework of mechanics of a deformable solid body.

For polymers at high loading rates and at amplitudes of force impact that do not let to viscous or brittle destruction elastic types of deformations are typical [33]. The plasticity mechanisms of polymers develop at sufficiently long exposure times (of the order of seconds and longer), and at force loading during the time of the order of microseconds and sufficiently large amplitudes, the stiffness of the material increases and, consequently, the energy required for deformation increases as well. It is claimed [34-35] that a polymer even in in liquid state can exhibit elastic solid body properties with high strength when is subjected to a short-term load.

From the duration of electromagnetic processes in the diode and the determination of the time of the substance flows impact on the PT, it follows that the duration of the force impact on the tube is not more than 2 microseconds, i.e. the load is short-term. This testifies in favor of elasticity of the model, in which elastic processes would not have time to be realized, and consideration of elastic processes would lead to the need for even higher values of energy impacting on the PT within its same final states.

The flows of the substance acting on the tube were simulated by applying unsteady pressures to the finite element tube model surfaces, which were subjected to such influences according to the location of the PT in the diode (Fig. 8).

In the calculations we used data on composition and velocities of particle flows obtained from optical spectra.

The front of pressure pulse on PT is formed by a flux of light elements and elements with middle atomic masses.
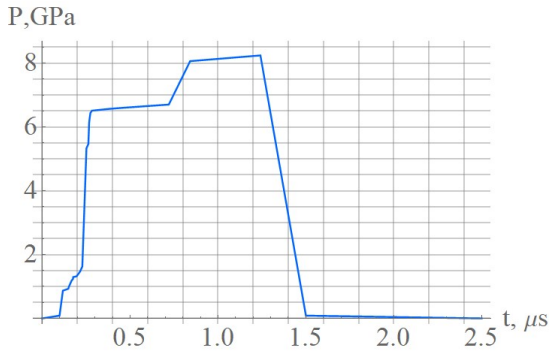
Fig. 9. Typical shape of pressure impulse on PT

Following these elements, next to approach the surface of a tube are heavy elements which then form the maximum pressure.

The flows of heavy elements are propagating near the PT surface in the medium formed from earlier approached flows, wherein the pressure is damped and the curve of the pressure on the tube surface drops at the final stage. The duration of this process is less than 2 microseconds and front about 100 ns.

In conditions of diode chamber and electromagnetic fields formed in it the fluxes of particles with different masses form two impacts - to the end face of the tube and to the inner surface of the tube.

The lighter elements reach the surface of the tube along curved trajectories, while the heavy ones along almost rectilinear paths. During the time of about 1.5 microseconds the hydrodynamic pressure pulse of 9 GPa consisting from components of heavy elements is formed at the end of the tube. At the same time, depending on the experimental conditions, almost all studied components find themselves in the region of the tube's cavity.

Upon reaching the change of PT shape in the model which is well consistent with the deformations observed during the experiments, the process of minimizing the received PT energy took place. For this purpose, the initial configuration of the loads was subjected to variations in which a decrease in the acquired PT energy preserved the type of deformation under consideration.

In the elastic approximation, there is no energy dissipation and during the exposure the energy of the tube consists of two components - deformation and kinetic. The kinetic energy of the tube is the energy of motion of its constituent parts irrespective of whether the center of mass moves or rests.
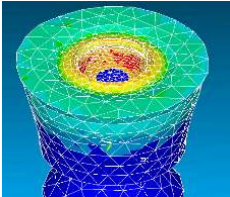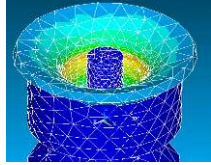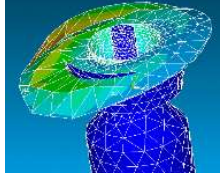
Comparison of PT shapes after exposure in the experiment and results obtained in the simulation are shown in Table 1.
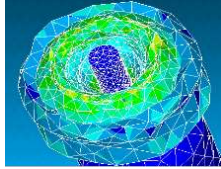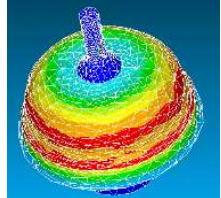
The right column shows the minimum flow energy values required to achieve the appropriate PT shape.

In the course of dispersal, the fluxes of heavy elements

have almost isotropic nature of dispersal and, consequently, a fraction of this flux corresponding to solid angle of the tube from the initial product dispersal sphere enters the tube cavity.

Table.1. Comparison of experimental and simulational final states of PT

| PT states in the experiment	PT states by simulation	kJ
		10.7
		16.4
		18
		32
		54

According to the measurement data, heavy elements account for ~2/3 of the optically measured fraction of the energy of the explosion products flux, so we can simply estimate that the energy delivered to the tube, taking into account the solid angle of the tube end, is 2.4 times less than the flux energy. Thus, in order for 40-50 kJ to be delivered to the tube region, as previously estimated, it is necessary for about 90-120 kJ to be released in the explosion region.

The use of plasma opening switch in the SING unit allowed to obtain the conversion of only a few percents of the energy of the capacitive storage into the energy of the electron beam, and the energy efficiency according to the evaluation of the cathode system deformation results in values in the range from 2 to 3, at the same time the released energy in relation to the driver (electron beam) energy turns out to be quite high and can reach values of the order of 10^2

4. ShAD unit and target explosion energy

In order to increase unit's and explosion energy's stability, the ShAD unit was designed with high voltage pulse amplitude greater than MV and currents of the order of 200 to 300 kA based on a DFL. A sketch of the ShAD unit is shown in Fig. 10.

High currents in the unit allow to obtain critical values of current [36] on the surface of the target with radius in a few millimeters and, therefore, capture a sufficiently large mass of matter in a non-linear wave to the center [7]. The explosion is initiated in the central region of the target, and products of its explosion are flown in all directions with velocities of about 10^7 cm/s.
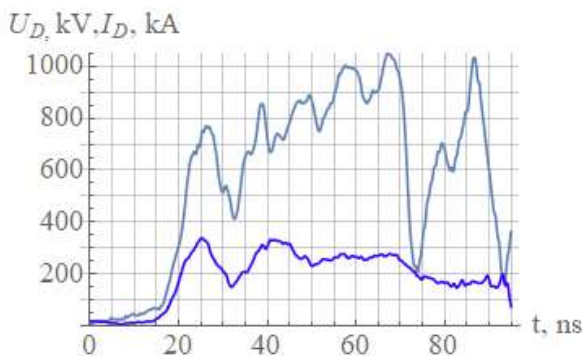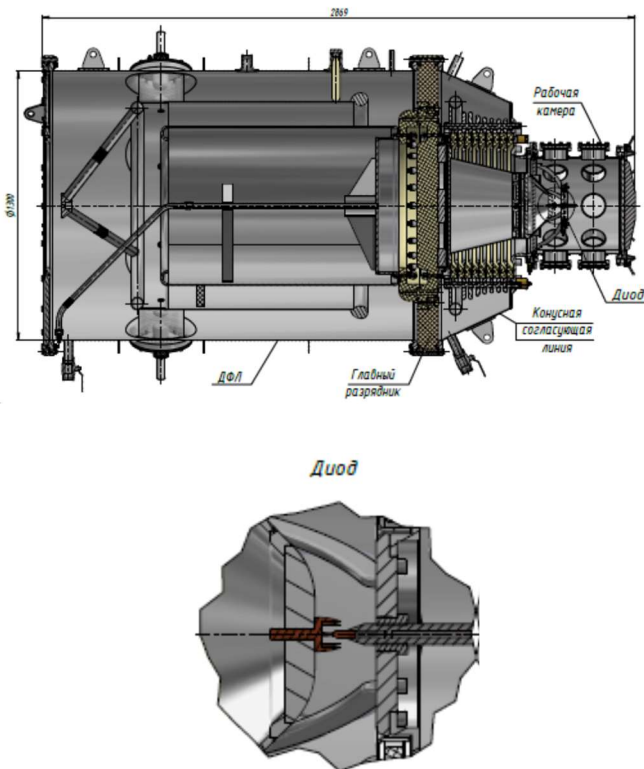
Fig.10. *Sketch of the DFL and diode of the ShAD unit. Typical oscillograms of current (lower curve) in the electron beam and voltage (upper curve) on the diode (experiment number 41317) on the bottom.*

The velocities of explosion products were measured using optical methods:

- Using Doppler's spectral line broadening
- By recording the time of reaching the optical radiation of three points located at different distances from the explosion center

In addition, optical imaging of the explosion process was carried out.

In processing the measured optical spectra standard spectral line contours were used [37,7]. An example of the optical spectrum from the explosion region is shown in the figure in Table 2.

Table 2. *Composition of dispersed flows from the center of the plumbum target and the optical spectrum used to reconstruct ion numbers and their velocities for experiment 41250*

Element	10^7cm/s	%
H		2.15
C	0.263	1.48
B	0.742	0.72
Na	0.524	1.38
Al	0.222	2.03
Ca	0.540	1.84
Ti	0.442	1.56
Cr	0.251	0.56
Mn	0.321	2.26
Fe	0.501	5.74
Cu	1.040	10.39
Zn	0.525	8.67
Hf	0.402	0.89
Pb	0.914	60.34
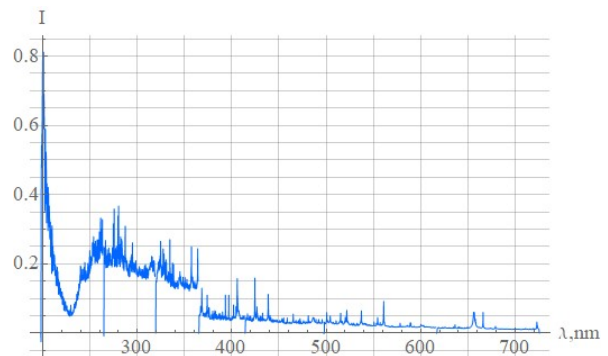
At first, an operation to exclude the contributions made by instrumentation function of the device was performed, the data on which were obtained in the result of the mercury lamp spectrum measurements. Then the measured spectrum was decomposed into its components, i.e. into separate spectral lines. During the processing, the width and shape of the line were varied until an optimal concurrence between the total

contour of spectral lines and experimental points was reached. The results of measurements of the composition of the dispersed fluxes in the experiment with a hafnium target are presented in Table 2.

The average particle velocity of this flux during this experiment obtained using the Doppler's line broadening of the optical spectrum was about 6. 10^6 cm/s. In the experiments, the flux velocities vary, but mainly lie in the range from 2.0 10^6 cm/s to 1.9 10^7 cm/s.

The velocities of the dispersed flows were also estimated using the time-of-flight method, which showed values close to those obtained by Doppler's broadening.

The radiation from the given points was recorded using a monochromator (see Fig. 11) and knowing the distance between the measuring points and obtained time intervals of the optical signal appearance we get the velocities of the target explosion products flux propagation.
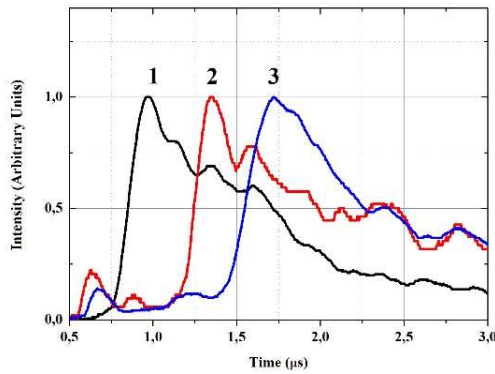
Fig. 11. *Intensity of the light registered using a monochromator (NP250-2M) at different points and calculation of the target explosion products velocities.*
$u_{1-2}=0,9cm/0,379\mu s=2,38*10^6cm/s;$
$u_{1-3}=1,8cm/0,750\mu s=2,40*10^6cm/s;$
$u_{2-3}=0,9cm/0,371\mu s=2,42*10^6cm/s.$

A small part of the explosion product fluxes at the flyout from the target center (proportional to the cathode element solid angle) interacted with the cathode elements and performed mechanical work to deform it.

Figure 12. shows typical states of the cathode - anode system before and after the explosion in the area of the target center.

Fig. 12. **Sketches of cathode - anode system before explosion (left) and after explosion (right).** *The cathode-anode system as part of the unit is shown in the sketch, see Figure 4.*

The key role in the transparency of the medium for optical observations is played by Rosseland free path for the light quantum in the medium [38]:

$$ l_p = \frac{10^{22}\,T^{7/2}}{z\,n^2} \begin{cases} 480\,z^{-2} \\ 1.3\left(z^2 + z\right)^{-1} \\ 4.4\left(1 + z\right)^{-2} \end{cases} $$

where *T* is for plasma temperature in degrees, *z* is for degree of ionization of atom emitting a quantum of light, *n* is for density of ions in the medium of quantum propagation, one of three possibilities after the curly bracket represents features of realizations of light absorption in the medium (free-free transition of photons, single ionized, multiply ionized atoms). If the medium's size exceeds the value of the Rosseland free path for the light quantum emitted by the atom, the quantum is absorbed by the medium and an optical device, of course, does not register it.

The ion density for the spherical expansion approximately decreases quadratically with the radius. Optical measurements in our experiment integrate the whole process from the beginning of the explosion to the moment of contact of the expansion sphere with the walls of the diode chamber. In the course of this process the ion density decreases to the limits determined by the maximum possible radius of the expansion sphere. For the initial moment of the dispersal we obtain Rosseland free path, which is negligibly small in comparison with the radius at which the process is observed – such radiation cannot be recorded.

The ratio of the energy E_0, contained in the transparent layer to the energy E_s of the exploded layer with energy approximately uniformly distributed on it will be equal to the ratio of the volumes of these layers. In the present case the energy of the explosion is greater than the one observed optically and E_s / E_0 is in the range from 300 to 3000
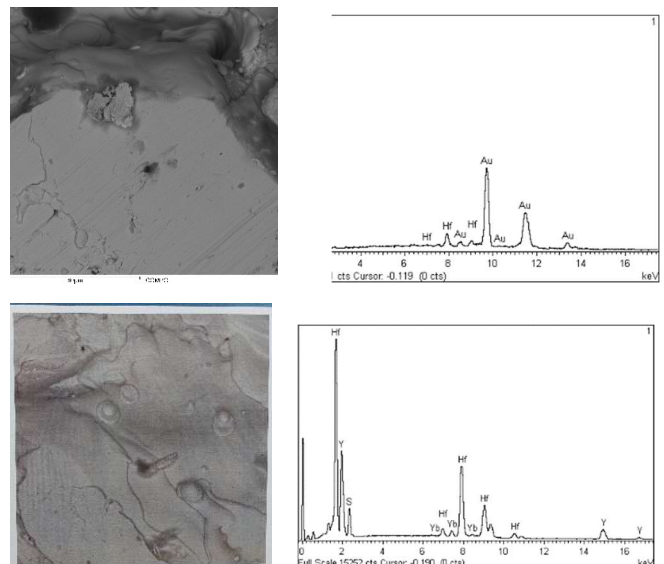
Fig. 13. **Macroscopic accumulations of Au (top) and Yb and Y (bottom elements on the target's remnants after the explosion of a hafnium target.** *A picture taken from the electron microscope on the left, the corresponding sections of the X-ray spectrum on the right.*

The explosion processes in the diode were also recorded using high-speed CCD-cameras. From the obtained images it was possible to estimate some representative times of the processes: it took about 50 nanoseconds for expanding cloud which was formed from the explosion of the target to pass through the gap of 1 cm, and the copper cathode elements bending took less than 500 nanoseconds.

Although the main efforts in the facilities have been made to recording the explosion energy and thorough analysis of fusion products (as in the case of low-power RVD-type facilities), fusion products in the form of rare elements had also being registered (see Fig. 13), which indicates the processes in the target at the nuclear level.

Taking into account that the mass loss during explosion from different experiments ranges from 0.1 g to 0.9 g, and the velocity of this mass is in the range $(0.5-1.9) \cdot 10^7$ cm/s, the target explosion products energy can be estimated in the average value from 300 kJ to 1 MJ

5. Conclusion

Experiments on nuclear fusion in high-current diode targets in Proton-21, which were started at small units with electron beam energy about 0.1 kJ and with target masses about 10 milligrams [25] were continued at units with beam energy about 10 kJ and with target masses about grams.

In experiments at such low-power units, fusion products in a wide range of nuclear masses were recorded [7,25].

At the high-power SING and ShAD units, it was possible to reach the release of energy during an explosion, that occurred in the center of the target after the processes initiated using electron beam on its surface.

The primary storage energy at the input of the SING and ShAD units ranged in 30 kJ-55 kJ, and the explosion energy released in the target center, estimated using optical measurements presented in this paper, ranged from 300 kJ to 1 MJ. Thus, the energy efficiency Q of the Proton-21's units was brought to an average values in the range of 10 to 30.

Acknowledgements

References

[1] Wesson, John; et al (2004). *Tokamaks*. Oxford University Press. ISBN 0-19-850922-7.

[2] J. Duderstadt and G. Moses, Inertial Confinement Fusion (Wiley, New York, 1982).

[3] Olson, C. L., "Z-Pinch Inertial Fusion Energy," in Landholt-Boernstein Handbook on Energy Technologies (Editor in chief; W. Martienssen), Volume VIII/3, Fusion Technologies (Edited by K. Heinloth), Springer-Verlag (Berlin-Heidelberg) in press (2004). [Includes an extensive list of references.]

[4] R.W. Bussard, "Some Physics Considerations of Magnetic Inertial-Electrostatic Confinement: A New Concept for Spherical Converging-flow Fusion," Fusion Technology 19, 273 (1991).

[5] A.V. Pashchenko, B.N. Rutkevich. Dynamics of transitions between the stationary states in diode // Radiotekhnika i Elektronika. 1979, v. 24, № 1, p. 152-157 (in Russian).

[6] A. Pashchenko, V. Ostroushko. Electron flow dynamics in resistive gap // Problems of Atomic Science and Technology. Series "Beam dynamics". 2017, № 6(112), p. 58-62.

[7] S. Adamenko, Selleri, van der Merwe, "Breakthroughs Experiment and Theory," Springer, Berlin (2007)

[8] Adamenko S.V. Method and device for compressing a substance by impact and plasma cathode, International Patent EP1464210 B1, 27, September 2006.

[9] E. M. Burbidge, G. R. Burbidge, W. A. Fowler, and F. A. Hoyle, Rev. Mod. Phys. 29, 547 (1957).

[10] S. L. Shapiro, S. A. Teukolsky, *Black holes, white dwarfs and neutron stars* (Wiley-Inters.cience, New York, 1983)

[11] S. Adamenko et al, Mechanism of synthesis of superheavy nuclei via the process of controlled electron-nuclear collapse. *Foundations of Physics Letters*, Vol. 17 No. 3. June, p. 203- 233 (2004)

[12] S. Adamenko et al, Evolution of annular self-controlled electron-nucleus collapse in condensed targets. *Foundations of Physics* **34**, No. 11. Nov, p. 1801-1831 (2004)

[13] S. Adamenko et al, Neutronization and protonization of nuclei: two possible ways of the evolution of astrophysical objects and the laboratory electron-nucleus collapse. *Foundations of Physics Letters* **19**, No.1, February, p. 21-36 (2006)

[14] Vysotskii V., Adamenko S. Correlated states of interacting particles and problems of the Coulomb barrier transparency at low energies in nonstationary systems. Tech Phys. 2010; 55:613621

[15] S. Adamenko, V. Vysotsky. Peculiarities of formation and application of correlated states in nonstationary systems at low energy of interacting particles. Journal of Experimental and Theoretical Physics — JETP, 2012, volume 141, no. 2., pp. 276-287.

[16] S. Adamenko, V. Novikov, A. Pashchenko, I. Shapoval. Nonlinear self-consistent processes with sharpening, quasi-stationary fractal plasma-field structures and the concept of the relationship between macro- and microscopic processes in dense plasma. Advances in modern radio electronics 11, p. 55-65 (2005).

[17] S. Adamenko, N. Bogolubov, V. Novikov, S. Kruchinin. Self-organization and nonequilibrium structures in the phase space, *International Journal of Modern Physics B,* Volume 22, Issue

3, pp. 2025-2045 (2008).

[18]   S. Adamenko, V. Bolotov, V. Novikov, Control of multiscale systems with constraints Interdisciplinary Studies of Complex Systems, Vol. 1, No. 1 (2012) 33–54.

[19]   S. Adamenko, V. Bolotov, V. Novikov, Control of multiscale systems with constraints Interdisciplinary Studies of Complex Systems, Vol. 1, No. 1 (2012) 55–77.

[20] Adamenko SV. Method and device for compressing a substance by impact and plasma cathode, International Patent EP1464210 B1, 27, September 2006.

[21]   Samarskii A., Galaktionov, V. Kurdyumov, S., Mikhailov A. «Blowup in Quasilinear Parabolic Equations». Berlin: Walter de Gruyter, 1995.

[22]   A. Adamenko, S. Adamenko, E. Bulyak. Experimental studies of excitation of a converging density wave in a cylindrical anode of a high-current diode. Letters Tech. Phys., vol. 31, issue 10, p. 24-29 (2005).

[23]   S.V. Adamenko, A.S. Adamenko, A.A. Gurin and Yu. M. Onishchuk. Track measurements of fast particle streams in pulsed discharge explosive plasma. *Radiation Measurements* **40**, No.2-6, November, p. 486-489 Proceedings of the 22nd International Conference on Nuclear Tracks in Solids (2005).

[24]   S. Adamenko, A. Adamenko, A. Gurin and M. Kuzmenko. Proton and alfa – radiation of the Micro-Pinch with Boron-Containing Target. Acta Polytechnica (2005).

[25]   S. Adamenko et al, Exploring new frontiers in the pulsed power laboratory: Recent progress. Results In Physics, 5, 2015, p 62-68.

[26]   S. Adamenko, V. Novikov., A. Pashchenko, V. Petukhov, I. Shapoval. Application of the finite element method to the modeling of large deformations of dielectric structural elements. Impulse processes in continuum mechanics. Proceedings of the International Scientific Conference, August 17-21, 2009, Nikolaev, p. 111-113 (2009).

[27]   V. Vysotsky, S. Adamenko, M. Vysotsky, Acceleration of low energy nuclear reactions by formation of correlated states of interacting particles in dynamical systems? Annalsof Nuclear Energy, Vol. 62, p618-625 (2013)

[28]   K.K. Gudima, A.S. Parvan, M. Ploszajczak, and V.D. Toneev *Nuclear Multifragmentation in the Non-extensive Statistics - Canonical Formulation*. Phys. Rev. Lett. 85 (2000) 4691-4694; Preprint GANIL-P-00-16, 2000. 4pp; nucl-th/0003025

[29]   K.K. Gudima, A.S. Parvan, V.D. Toneev. Caloric curve and multifragmentation in collisions of heavy ions with intermediate energies. *Physics of Atomic Nuclei*, 1999, vol. 62, no 9 p. 1593-1604.

[30]   J. Dechargé, J.-F. Berger, M. Girod, K. Dietrich, Bubble and Semi bubbles as a new kind of superheavy nuclei, Nuclear Physics A 716(2003), pp. 55-86

[31]   T. Maruyama, K. Niita, K. Oyamatsu et al., Quantum molecular dynamics approach to the nuclear matter below the saturation density, Phys. Rev. C, Vol 57, Number 2, p. 655

[32]   W. Greiner, Exotic nuclei: from super-heavies to hyper and antimatter, Nuclear Physics 64(6), 1191 (2001).

[33]   Kabanov V. Encyclopedia of polymers. T. 2, 1974, 516 p.

[34]   Azarov V. Chemistry of synthetic polymers, 1976, 288 p.

[35]   Bartenev G. Physics of polymers, 1990, 433 pp.

[36]   O. Manuilenko, I. Onishchenko, A. Pashchenko, I. Pashchenko, V. Yuferov. Current flow dynamics in plasma opening switch // Problems of Atomic Science and Technology. Series: "Plasma Electronics and New Methods of Acceleration". 2021, №4 (134), p. 6 – 10.

[37]   R. H. Huddlestone and S. L. Leonard (Eds.) *Plasma Diagnostic Techniques* (Academic Press, New York, 1977).

[38]   Alexandrov A., Rukhadze A. (1974). High-current electric-discharge light sources. Physics Uspekhi (Advances in Physical Sciences), 112 (issue 2): 193-230.